Title

Specific Absorbed Fractions for Spontaneous Fission Neutron Emitters in the ICRP Reference Pediatric Voxel Phantom Series.

Journal

Health Physics, 123(4)

Authors

Griffin, Keith
Eckerman, Keith
Jokisch, Derek
et al.

Publication Date

2022-10-01

DOI

10.1097/HP.0000000000001594

Peer reviewed

HHS Public Access

Author manuscript

Health Phys. Author manuscript; available in PMC 2023 October 01.

Published in final edited form as:

Health Phys. 2022 October 01; 123(4): 278–286. doi:10.1097/HP.0000000000001594.

Specific absorbed fractions for spontaneous fission neutron emitters in the ICRP reference pediatric voxel phantom series

Keith T. Griffin[1,2], **Keith F. Eckerman**[3,7], **Ryan P. Manger**[4], **Derek W. Jokisch**[5,7], **Wesley E. Bolch**[6], **Nolan E. Hertel**[1]

[1]George W. Woodruff School of Mechanical Engineering, Georgia Institute of Technology, Atlanta, GA

[2]Division of Cancer Epidemiology and Genetics, National Cancer Institute, National Institutes of Health, Rockville, MD

[3]Environmental Sciences Division, Oak Ridge National Laboratory, Oak Ridge, TN

[4]Department of Radiation Medicine and Applied Sciences, School of Medicine, University of California San Diego, San Diego, CA

[5]Department of Physics and Engineering, Francis Marion University, Florence, SC

[6]J. Crayton Pruitt Family Department of Biomedical Engineering, University of Florida, Gainesville, FL

[7]Center for Radiation Protection Knowledge, Oak Ridge National Laboratory, Oak Ridge, TN

Abstract

Specific absorbed fractions (SAFs) are a key component in the workflow of internal exposure assessment following the intake of a radionuclide, allowing quick conversion of particle energy released in a source region to the expected absorbed dose in target regions throughout the body. For data completeness, SAFs for spontaneous fission neutron emitters are currently needed for the recently-adopted ICRP reference pediatric voxel phantom series. With 77 source regions within each reference individual and 28 radionuclides decaying via spontaneous fission, full Monte Carlo simulation requires significant computation time. In order to reduce this burden, a novel method for neutron SAF estimation was undertaken. The Monte Carlo N-Particle version 6.1 (MCNP6) simulation package was chosen to simulate the ^{252}Cf Watt fission neutron spectrum originating from 15 source regions in each phantom; dose estimation within 41 target tissues allowed for assessment of the SAF value for each source-target pair. For the remaining source regions, chord length distributions were computed using MATLAB code to determine the separation between the source-target pairs within the pediatric phantom series. These distance distributions were used in conjunction with a ^{252}Cf neutron dose point kernel calculated in soft tissue, which was modified to account for the source region's depth from the surface of the body. Lastly, the ^{252}Cf SAF dataset was extended to the other 27 spontaneous fission neutron emitters based on differences in the Watt fission spectrum parameters of each radionuclide. This methodology has been shown to accurately

Corresponding Author: Nolan Hertel, PhD, Professor, George W. Woodruff School of Mechanical Engineering, 770 State St. NW; Atlanta, GA 30313, Boggs Building, Room 3-84, 404-894-3601 (Office), nolan.hertel@me.gatech.edu.

estimate spontaneous fission neutron SAFs to within 20% of the Monte Carlo estimated value for most source-target pairs in the ICRP reference pediatric series.

Keywords

internal dose; ICRP; phantom; Monte Carlo

1 Introduction

Following the intake of a radionuclide, comprehensive dosimetry methods are required for the triage and dose management of the exposed person. Extensively researched biokinetic models describe how various radionuclides travel and reside within the organs of an individual (Paquet et al 2015, 2016, 2017, 2019). The biokinetic compartments become “sources” of emitted radiations that deliver dose to “target” regions of the body. This line of thought is reflected within the internal dosimetry schema first standardized by the Society of Nuclear Medicine (Loevinger and Berman 1968, Loevinger et al 1991), which was later conformed to the nomenclature of the International Commission on Radiological Protection (ICRP) (Bolch et al 2009). Within this formalism, the internal dosimetry process is informed by an important quantity termed the specific absorbed fraction (SAF), which provides the fraction of energy emitted in a source region that is absorbed in a target region per unit mass of target region. SAF values for reference individuals are a pre-calculated and tabulated quantity for a set of energies of the emitted radiations in this formalism, found through Monte Carlo (MC) radiation transport simulation to make the conversion from time-integrated activity of the radionuclide into organ absorbed dose.

The ICRP has previously published SAFs for the reference adult male and female within ICRP Publication 133 (Bolch et al 2016). These SAFs are computed using the whole-body adult voxel phantom series of ICRP Publication 110 (ICRP 2009) and supplemented with other models for charged particles in tissues of the alimentary tract, respiratory tract, and the skeleton. These tabulated SAFs are for monoenergetic photons, electrons, and alpha particles. S-values for specific radionuclides may be constructed from these monoenergetic data by interpolation using the energies of these radiations taken from the nuclear decay data of ICRP Publication 107 (ICRP 2008). In addition to monoenergetic radiations, ICRP 133 also includes SAFs from fission-spectrum neutron spectra for the 28 radionuclides of ICRP 107 that decay via spontaneous fission. Recently, the ICRP has adopted a new series of pediatric voxel phantoms within ICRP Publication 143 to represent the reference pediatric male and female anatomy at five ages (Bolch et al 2020). Task Group 95 of ICRP Committee 2 is currently addressing the need for the development of complementary age-dependent SAFs. Under the scope of these efforts, the purpose of this work is to describe the calculation methodology that was used to estimate spontaneous fission neutron SAFs for the new ICRP reference pediatric phantom series. The methodology is similar to but improved upon that which was previously employed in deriving the adult spontaneous fission neutron SAFs of ICRP 133.

2 Materials

2.1 ICRP reference pediatric phantom series

The ICRP reference pediatric phantom series is a ten-member collection, consisting of male and female anatomies at ages newborn (at birth), 1-year-, 5-years-, 10-years-, and 15-years-old; these phantoms share the same anatomy between sexes at ages 10 and below, apart from the sex-specific organs and the location of the urinary bladder. The ICRP reference series originates from the most recent generation of phantoms called hybrid phantoms, where the delineations of organ and tissue contours are defined using polygonal meshes and non-uniform rational B-spline surfaces within computer-aided design software (Xu 2014). For implementation into current MC simulation packages, these mesh phantoms were converted and published in voxel format, as shown in Figure 1, using the processes originally described in Lee *et al.* (Lee et al 2007). In voxel format, anatomical information is contained within a three-dimensional matrix of numerical organ identifier (ID) values, where each ID represents a specific organ or tissue within the reference phantom, with age-dependent elemental compositions and densities as provided by ICRP Publication 89 (ICRP 2002) and International Commission on Radiation Units and Measurements (ICRU) Report 46 (ICRU 1992). Physical voxel resolution and array dimensions for these phantoms can be found in Table 4.1 of ICRP Publication 143. The current ICRP internal dosimetry calculation uses 79 source regions and 43 target regions (77 sex-specific source regions and 41 sex-specific target regions per phantom). ICRP Publications 110 and 143 provide tables which map the source and target regions to the numerical organ ID values in the reference voxel phantoms. To cover each source and target region combination results in 3,157 source-target pairs within each phantom that require an SAF calculation.

2.2 Monte Carlo simulation package

The Monte Carlo N-Particle version 6.1 (MCNP6) simulation package was chosen to perform the radiation transport of spontaneous fission neutrons for those SAFs calculated through full MC simulation in this work (Pelowitz 2013). Neutron cross-section data tabulated at 293.6 K were retrieved from the ENDF/B-VI.6 library (U.S. Evaluated Nuclear Data File/B Version VI Release 6). When available, neutron cross sections were used for elements in their natural isotopic abundance; otherwise, cross-sections were specified for elements using their isotope of largest abundance (Conlin et al 2014). The S(α,β) treatment available in MCNP6 for hydrogen bound in light water was used to account for the upscatter of thermal neutrons.

3 Methodology

The MC calculation of SAFs within a voxel phantom started with the sampling of particles at randomly selected positions within the source region. The probability of one of the source voxels being sampled as a starting location was based on its fraction of the total organ mass. For most source regions in the ICRP reference series, the tissue composition and density are uniform throughout; one such example is the liver, which only has one organ ID value. In this case, a uniform source sampling distribution was used such that all liver voxels have an equal probability of being chosen. For source regions with varying density, such as the

lungs, a mass density-weighted sampling distribution was used such that the probability of choosing a voxel was in proportion to its mass density relative to the other source voxels. Once a voxel was selected, the simulated neutron history began at a randomly selected point within the voxel.

There are also several important source regions that are not distinctly defined within the phantom series, instead being implicitly distributed throughout the body's defined organ and tissue sites; these distributed regions can be subdivided into two groups: blood and bone. An overview of the source sampling procedure used in this work is provided in Table 1 for SAF calculation for the blood and bone source regions of the ICRP pediatric reference phantom series. In both the pediatric and adult reference series, bone sites are delineated into cortical, medullary cavity, and spongiosa regions. For some bone source regions, such as the cortical bone marrow, density-weighted sampling of the segmented cortical bone sites is possible; for more complicated source regions, such as the active and inactive marrow, external data on the distribution of the source region within each bone site must be incorporated. The age-dependent fractional tissue weights of bone volumes and marrows within the reference phantom series are provided by Tables 3.3-3.8 of ICRP 143. Blood is also a unique source term. Not only is blood in homogeneous form within the phantom as segmented blood vessels and contents of the heart; it is also dispersed throughout all tissues of the body. The age-dependent blood content proportions within the segmented blood vessels and major organs of the body, originally developed by Wayson et al. (Wayson et al 2018), are given by Table 4.3 of ICRP 143. Calculation of the SAF for blood as a source was thus performed in two steps. One SAF simulation was performed for blood using a weighted sampling of the segmented blood vessels of the body based on their contained percentage of total segmented blood. This SAF was then summed with other source region SAFs of the body, which are already calculated by this work, to create a weighted sum estimate of the blood SAF based on each source region's blood content.

An initial investigation into the use of MCNP6 to compute spontaneous fission SAFs within the ICRP reference pediatric series found that by simulating 20 million spontaneous fission neutron histories for each source region, nearly all SAFs were estimated to within 10% uncertainty. At roughly 20 CPU-hours per simulation, full MC simulation of all 77 source regions, within the 10 phantoms, and for all 28 radionuclides would require over 400,000 CPU-hours of runtime. Instead, in similar fashion to what was previously performed for the adults in ICRP 133, full MC simulation was only performed for 15 source regions that were deemed most important to internal dosimetry from a heavy metal intake: the liver, lungs, digestive system contents (stomach, small intestine, right colon, left colon, and rectosigmoid colon), kidneys, trabecular bone, trabecular bone marrow, cortical bone, cortical bone marrow, testes, ovaries, segmented blood vessels, and the miscellaneous soft tissues of the body (i.e. adipose tissue and muscle, which are needed for blood source SAF estimation). Additionally, full simulations were only performed for one of the 28 radionuclides, ^{252}Cf, which was chosen based on its high spontaneous fission branching fraction and significant worldwide abundance. The remaining SAFs, 62 source regions for ^{252}Cf and all source regions for the remaining 27 radionuclides, were determined by scaling the ^{252}Cf SAFs as detailed below.

3.1 Monte Carlo simulation approach to ^{252}Cf SAF estimation

For definition of a source term within MCNP6, the location of the starting particle must be given in a manner as described in the previous section. Source definition cards were created for each source region of the phantom, providing the voxel indices within the three-dimensional phantom matrix and the relative probability to start a particle within that voxel. Particles were started randomly within the chosen voxel with isotropic direction and energy based on the ^{252}Cf Watt fission spectrum parameters given by ICRP 107. Target region dosimetry within MCNP6 was performed for most target tissues using the +F6 tally, corresponding to a track-length heating tally (in units MeV/g). These tallies were converted into an SAF (kg^{-1}) by dividing by the average emitted neutron energy per fission for ^{252}Cf (2.3057 MeV) and converting to $kilograms^{-1}$. The mass of the target regions within the MC simulation contained no blood; to correct for this, mass ratios of tissue to tissue plus blood content were used to adjust the final SAFs. These ratios were computed using the mass of the targets in the voxel phantom to the reference target masses inclusive of blood. For the adult the reference masses inclusive of blood are provided in Tables A.1 and A.2 of ICRP Pub. 133. For the pediatric series, blood inclusion is based on an age-distribution model provided in Wayson et al (2018). For the active marrow (red bone marrow) and shallow marrow (bone endosteum) targets, the neutron and photon fluences were computed by using a track length fluence estimator (F4 tally) at 25 marrow-containing bone sites of the phantoms. Neutron fluence-to-dose response functions for the ICRP reference adult male were used to convert neutron fluence to active marrow and shallow marrow dose at each site (Bahadori et al 2011); neutron dose response functions for the pediatric series are not available. Photon fluences, created through neutron-gamma reactions within the body, were converted to active marrow and shallow marrow dose at each site through photon fluence-to-dose response functions, which are available for each pediatric phantom age and sex under a forthcoming ICRP Publication. Lastly, the known proportions of active marrow and shallow marrow within each bone site were used to make a weighted-sum estimate for the active marrow and shallow marrow absorbed dose to arrive at the SAF.

3.2 Point kernel approach to ^{252}Cf SAF estimation

For source regions not subject to MC simulation, a point kernel method was adopted, which converts the distance between source and target regions into an SAF. This conversion was made possible by determining the dose in soft tissue as a function of source-to-target separation within the body. The simulation geometry, as set up within MCNP6, is depicted in Figure 2 for the neutron SAF point kernel creation – a 15-centimeter radius soft tissue cylinder surrounded by air. A ^{252}Cf point source is centrally located within the cylinder model, with dose to the soft tissue tallied (+F6) within the varying radii outwards, as depicted by the many onion-like layers of the cylinder; dose was tallied at radii from 0 – 40 cm in 0.5 cm intervals, from 40-60 cm in 1 cm intervals, and from 60-100 cm in 5 cm intervals. 10 million histories were simulated, with resulting dose tallies calculated to within 3% statistical uncertainty.

This initial model, with the source started at the center of the cylinder, is shown on the left of Figure 2. While adequate for deep-seated regions of the body, the central source placement overestimates the SAF for a source region near the surface of the body; this is

because the model would overestimate the number of neutrons backscattering into the body from surrounding air. To account for this, five point kernel models were simulated within MCNP6: one with the ^{252}Cf point source term centered in the cylinder, and ones with 3 cm, 6 cm, 9 cm, and 12 cm transverse offset from the center, as shown in Figure 2. In this way, an appropriate neutron SAF kernel may be selected for a source region based on its depth within the body. Source region depths were determined for each phantom using a recently published methodology for determining the organ depth distribution within a voxel phantom (Griffin et al 2020). The depth distribution of a source organ in the body was determined on the transverse plane of the phantom, corresponding to the rotational (ROT) organ depth distributions described by the publication. An offset kernel was assigned to the source region based on the 25th percentile depth of the source organs in the ROT direction to the surface of the body (i.e., the 75th percentile closest organ voxel to the skin surface); validation tests proved this choice of the 25th percentile to perform the best at SAF estimation. This accounting for organ depth within the body in the SAF calculation approach was the novel improvement to an unbounded spherical point kernel assumed in the adult SAF methodology.

With a point kernel conversion available, knowledge on the distance between source and target regions can now provide SAF estimates. This source-target separation was computed using the organ depth distribution method described above, with distance calculated from one sampled position in the source region to another sampled position in the target region. 100,000 distances were computed for each source-target pair of the phantoms, resulting in a distribution of source-to-target distances binned at 1 mm intervals. From the relative number of histories within each bin, a weighted sum estimate of the SAF can be made using the appropriately offset point kernel to convert each distance to an SAF. The kernel was interpolated in between distance values using a PCHIP interpolator (Fritsch and Butland 1984). Individual bone sites were considered the targets for the active and shallow marrow, with their contributions to the chord length distribution weighted by each site's contained marrow fractions.

3.3 Extension approach to remaining radionuclides

At this stage, the SAFs for 3,157 source-target pairs defined in each ICRP pediatric phantom had been derived for the ^{252}Cf spontaneous fission neutron spectrum. This dataset of ^{252}Cf SAFs was extended to the other 27 radionuclides that undergo spontaneous fission based on the differences in each radionuclide's Watt fission spectrum. ICRP 107 (Table 2.5) provides the Watt fission spectrum parameters for the radionuclides. For each radionuclide, a dataset of neutron KERMA coefficients for soft tissue were integrated over the Watt fission spectrum to obtain a radionuclide-specific KERMA coefficient; these neutron KERMA coefficients in soft tissue have previously been tabulated (Howerton 1986). Normalization of the radionuclide-specific KERMA coefficient to that of the ^{252}Cf coefficient provides one factor for scaling the ^{252}Cf SAFs. Additionally, because the SAFs are derived through normalization to the average emitted neutron energy per fission, a second factor must be applied to adjust for these differences. Spectral-averaged radiation weighting factors, w_R, were also derived assuming the guidance of ICRP 103 (p 66). The SAF scaling factors and the radiation weighting factors for each radionuclide are summarized in Table 2.

3.4 Validation

Validation of the point kernel SAF estimation and extension processes described above was undertaken to determine whether the methodology was effective at providing accurate SAF estimates for the ICRP pediatric phantom series. The results for the 15-year-old male will be discussed, since it contains the largest source-target separation, representing the most difficult SAFs to estimate by this work. For validation of the ^{252}Cf SAFs estimated using the point kernel method, SAFs for source-target pairs already calculated through full MC simulation were re-estimated using the point kernel method; comparisons between SAFs found through full MC simulation and those estimated through the point kernel were made. For validation of the extension approach to other radionuclides, full MC simulation within MCNP6 was also performed for a small subset of the sources (liver, cortical bone, and trabecular bone) in the 5-year-old male for ^{238}U and ^{244}Pu using their unique Watt fission spectra. The results of these MC simulations were then compared to those SAFs estimated through the extension approach.

4 Results and Discussion

4.1 Californium-252 point kernel and chord length distributions

The results of the ^{252}Cf spontaneous fission neutron kernel calculation in soft tissue are shown in Figure 3, providing a conversion of source-target separation into an SAF for the five transverse depths within the model. Notably, the differences between the five kernels are greater at farther distances from source to target, indicating an increasing proportion of dose from scattered neutrons. At a source-target separation of 60 cm, the difference between SAFs of the central source location and the most external source location is nearly a factor of two. This result reinforces the value in including source region depth as a variable within the point kernel approach. Tabulated data on the neutron point kernels created by this work may be found in the Supplemental Digital Content (Table SDC1).

At the top of Figure 4, the chord length distributions are shown for two examples: the 15-year-old female liver source to stomach wall target separation and the 15-year-old male right colon contents source to thyroid target separation; at the bottom of Figure 4, the organ depth distributions are shown for these two source regions. In the example case of the 15-year-old female, the 25th percentile depth of the 15-year-old female liver was found to be 7.8 cm, leading to the selection of the 6 cm offset kernel (representing a source term roughly 9 cm within the surface of the body). As seen in Figure 4, the 15-year-old male right colon contents are much shallower within the body, with 25th percentile depth of 4.9 cm; this led to a selection of the 9 cm offset kernel. Interpolation of the offset kernels shown in Figure 3, in conjunction with the source-target chord lengths shown in Figure 4, allows for summed estimates of the SAFs to be made. The full dataset of calculated chord length distributions will be published in a future work.

4.2 Validation of ^{252}Cf SAF kernel and extension processes

In Table 3, differences in SAF values estimated using the point kernel methodology to those found through full MC simulation are shown. For the source-target pairs discussed in Table 3, the SAFs for ^{252}Cf were estimated to within 20% using the point kernel methodology.

Generally, this finding is also true for other source-target SAFs; 95% of all the SAFs calculated through full MC simulation in this study were estimated to within 20% by the point kernel method, and greater than 99% of the SAFs were estimated to within 50% of the MC value. For those SAFs with differences greater than 50%, the discrepancies are due to large statistical uncertainty from the MC simulation results themselves; in these few cases, the source-target separations are large, and the targets are small (i.e., the pituitary gland, tonsils, and eye lens targets), resulting in few source tracks reaching the tally volume within the MC simulation.

Validation of the extension of ^{252}Cf SAFs to those of two other radionuclides decaying via spontaneous fission – ^{238}U and ^{244}Pu – is shown in Table 4 for the 5-year-old male. These results show that the extension process made reasonable estimates of the SAFs calculated through full MC simulation. Although the ^{252}Cf source term transferred higher dose per source neutron in the MC simulations than ^{238}U or ^{244}Pu, the higher average fission neutron energy of ^{252}Cf compared to ^{238}U and ^{244}Pu (2.306 versus 1.687 and 1.765 MeV, respectively) resulted in comparatively lower SAF values. Overall, the SAFs for ^{238}U and ^{244}Pu were approximated to within 20% of the value found through full MC simulation for the entire subset of source-target pairs considered in this validation.

4.3 Study Limitations

In consideration of the very large SAF dataset required for the ICRP pediatric reference series, the main limitation to the completion of this work was the amount of computation time available to devote towards full MC simulation, which would have provided the most accurate methodology; nevertheless, the inaccuracies seen for the source-target SAFs estimated through the point kernel approach and extension methodologies are acceptable in the grand scheme of internal dosimetry. This is because the magnitude of the neutron dose estimates arising from spontaneous fission are quite insignificant compared to the alpha and fission fragment contributions, which dominate the total dose. For example, the absorbed dose to the liver from a uniform ^{252}Cf burden due to emitted alpha particles and fission fragments exceeds that due to spontaneous fission neutrons by more than two orders of magnitude; this is despite ^{252}Cf undergoing spontaneous fission in 3.09% of its nuclear transformations. The one exception to this would be the dose to the eye lens when the source region is the blood, as the eye lens is the only target region that does not contain blood. The contributions of the various radiations to the age-specific liver absorbed dose in the ICRP reference males are listed in Table 5; as expected, this dose decreases with increasing age due to greater self-shielding. Another limitation is in the use of a voxel phantom to represent the important dosimetric structures of the body. Some of these structures have very fine definition, being only a few microns thick (e.g., the radiosensitive stem cell layers of the gastrointestinal tract). The voxel phantom resolution is too coarse to properly capture this definition; instead, certain surrogacies were used as a best approximation (e.g., the entirety of the gastrointestinal wall as a surrogate for the stem cell layer). A list of the surrogacies used in this work can be found in the Supplemental Digital Content (Table SDC2).

5 Conclusions

Specific absorbed fractions for spontaneous fission neutron emission within the ICRP reference pediatric phantom series have been developed for the 28 relevant radionuclides of ICRP Publication 107. The methodology employed by this work followed similar procedure to the work performed for the adults, extended by novel computational methods with the pediatric phantoms. This resulted in a dataset of nearly one million SAFs, which have been tabulated for potential use in an upcoming ICRP Publication. The majority of these SAFs have been created using a unique point kernel estimation and extension methodology, saving a large quantity of computation time. This methodology has been shown to accurately estimate SAFs to within 20% of the Monte Carlo derived value for most source-target pairs.

Supplementary Material

Refer to Web version on PubMed Central for supplementary material.

Acknowledgments

This research was funded by the Environmental Protection Agency through the Center for Radiation Protection Knowledge at Oak Ridge National Laboratory. This work was also funded by the intramural program of the National Institutes of Health (NIH), National Cancer Institute, Division of Cancer Epidemiology and Genetics. The views of the authors do not necessarily reflect those of the U.S. government. Certain commercially available software is identified in this manuscript to foster understanding and should not be construed as a recommendation.

References

Bahadori AA, Johnson P, Jokisch DW, Eckerman KF and Bolch WE 2011 Response functions for computing absorbed dose to skeletal tissues from neutron irradiation Phys. Med. Biol 56 6873–97 [PubMed: 21983525]

Bolch WE, Eckerman K, Endo A, Hunt JGS, Jokisch DW, Kim CH, Kim K-P, Lee C, Li J, Petoussi-Henss N, Sato T, Schlattl H, Yeom YS and Zankl M 2020 ICRP Publication 143: Paediatric Reference Computational Phantoms Ann. ICRP 49 5–297

Bolch WE, Eckerman KF, Sgouros G and Thomas SR 2009 MIRD Pamphlet No. 21: A Generalized Schema for Radiopharmaceutical Dosimetry--Standardization of Nomenclature J. Nucl. Med 50 477 [PubMed: 19258258]

Bolch WE, Jokisch D, Zankl M, Eckerman KF, Fell T, Manger R, Endo A, Hunt J, Kim KP and Petoussi-Henss N 2016 ICRP Publication 133: The ICRP computational framework for internal dose assessment for reference adults: specific absorbed fractions Ann. ICRP 45 5–73

Conlin JL, Parsons DK and Gardiner SJ 2014 Listing of Available ACE Data Tables

Fritsch FN and Butland J 1984 A Method for Constructing Local Monotone Piecewise Cubic Interpolants SIAM J. Sci. Stat. Comput 5 300–4

Griffin KT, Cuthbert TA, Dewji SA and Lee C 2020 Stylized versus voxel phantoms: a juxtaposition of organ depth distributions Phys. Med. Biol 65 065007 [PubMed: 32059205]

Howerton RJ 1986 Calculated neutron KERMA factors based on the LLNL ENDL data file. Volume 27 (Lawrence Livermore National Lab., CA (USA)) Online: https://www.osti.gov/biblio/5934977

ICRP 2009 Adult Reference Computational Phantoms ICRP Publ. 110 Ann ICRP 39 1–166

ICRP 2002 Basic anatomical and physiological data for use in radiological protection: reference values ICRP Publ. 89 Ann ICRP 32 1–277

ICRP 2008 Nuclear Decay Data for Dosimetric Calculations ICRP Publ. 107 Ann ICRP 38

ICRU 1992 Report 46: Photon, Electron, Proton and Neutron Interaction Data for Body Tissues J. Int. Comm. Radiat. Units Meas os24 NP-NP

Lee C, Lodwick D, Hasenauer D, Williams JL, Lee C and Bolch WE 2007 Hybrid computational phantoms of the male and female newborn patient: NURBS-based whole-body models Phys. Med. Biol 52 3309–33 [PubMed: 17664546]

Loevinger R and Berman MA 1968 A schema for absorbed-dose calculations for biologically distributed radionuclides J. Nucl. Med 9

Loevinger R, Budinger TF, Thomas F and Watson EE 1991 MIRD Primer for Absorbed Dose Calculations revised edition (New York: Society of Nuclear Medicine)

Paquet F, Bailey MR, Leggett RW, Etherington G, Blanchardon E, Smith T, Ratia G, Melo D, Fell TP, Berkovski V and Harrison JD 2019 ICRP Publication 141: Occupational Intakes of Radionuclides: Part 4 Ann. ICRP 48 9–501 [PubMed: 31850780]

Paquet F, Bailey MR, Leggett RW, Lipsztein J, Fell TP, Smith T, Nosske D, Eckerman KF, Berkovski V, Ansoborlo E, Giussani A, Bolch WE, Harrison JD, and Authors on Behalf of ICRP 2016 ICRP Publication 134: Occupational Intakes of Radionuclides: Part 2 Ann. ICRP 45 7–349

Paquet F, Bailey MR, Leggett RW, Lipsztein J, Marsh J, Fell TP, Smith T, Nosske D, Eckerman KF, Berkovski V, Blanchardon E, Gregoratto D, Harrison JD, and Authors on Behalf of ICRP 2017 ICRP Publication 137: Occupational Intakes of Radionuclides: Part 3 Ann. ICRP 46 1–486

Paquet F, Etherington G, Bailey MR, Leggett RW, Lipsztein J, Bolch W, Eckerman KF, Harrison JD, and ICRP 2015 ICRP Publication 130: Occupational Intakes of Radionuclides: Part 1 Ann. ICRP 44 5–188 [PubMed: 26494836]

Pelowitz DB 2013 MCNP6 User's Manual Version 1.0

Wayson MB, Leggett RW, Jokisch DW, Lee C, Schwarz BC, Godwin WJ and Bolch WE 2018 Suggested reference values for regional blood volumes in children and adolescents Phys. Med. Biol 63 155022 [PubMed: 29999494]

Xu XG 2014 An exponential growth of computational phantom research in radiation protection, imaging, and radiotherapy: a review of the fifty-year history Phys. Med. Biol 59 R233–302 [PubMed: 25144730]

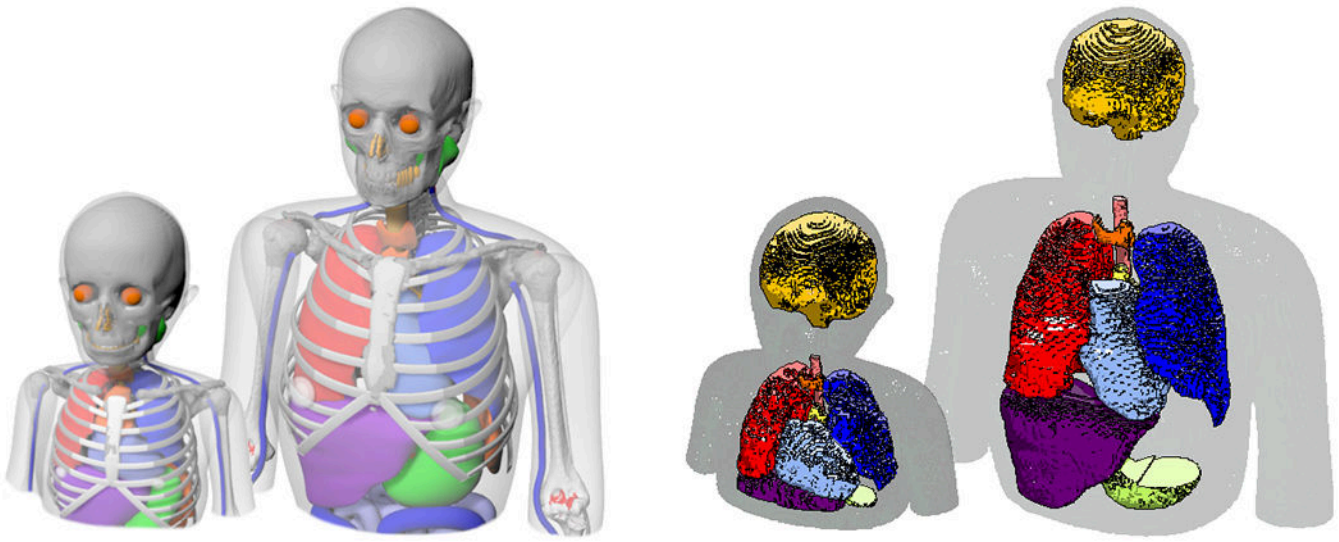

Figure 1:
(Left) Three-dimensional view of the 5-year- and 15-year-old male ICRP pediatric hybrid phantoms, representing reference anatomy, from left to right. (Right) Three-dimensional view of the voxelized versions of the 5-year- and 15-year-old male ICRP reference phantoms, with select organs and outer contour visualized, from left to right.

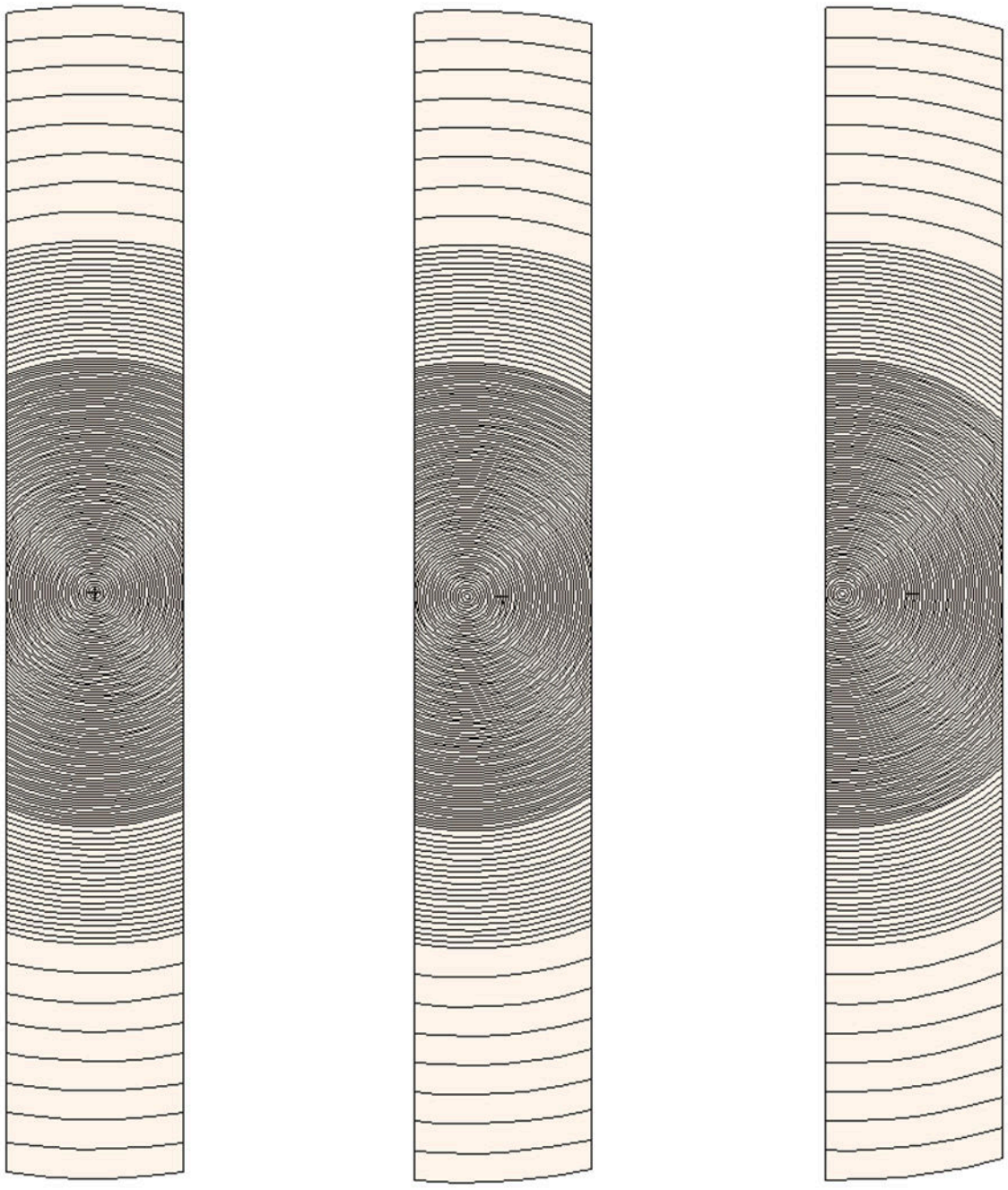

Figure 2:
Simulation geometries of the neutron SAF point kernel calculations: a soft tissue sphere bounded within a cylinder with radius 15 cm. Dose is tallied in varying spherical radii (0 – 100 cm) outwards from the source location, which is offset transversely from the center 0 cm (left), 6 cm from the center (middle), and 12cm from the center (right). Surrounding air confines the model with radius 150 cm.

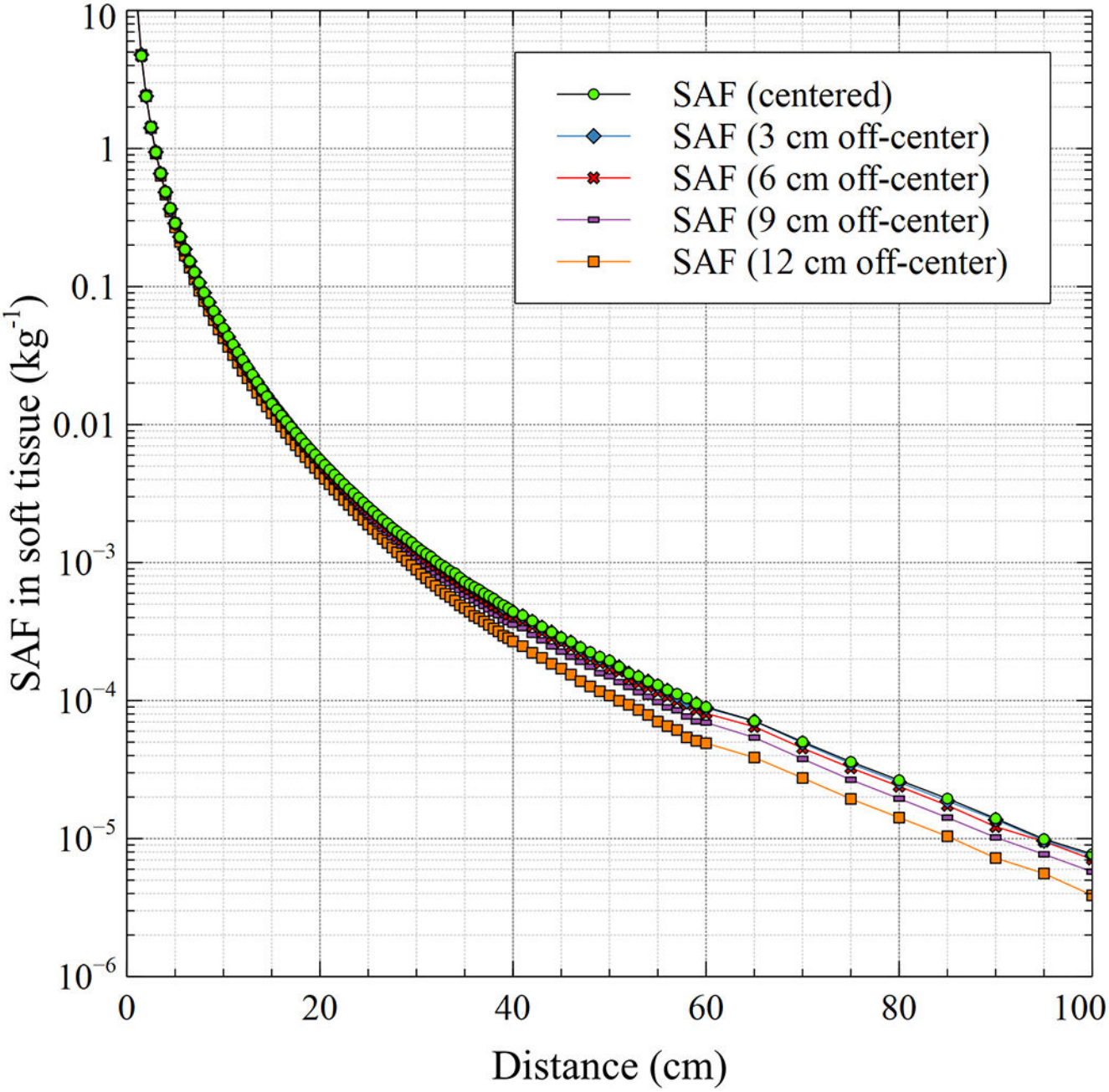

Figure 3:

Neutron SAF in soft tissue as a function of source-target separation (distance) for ^{252}Cf. Five SAF kernels are displayed, ranging from a central source location to a transverse source location offset by 12 cm from center, providing more accurate dose dependent on the source region's depth within the body.

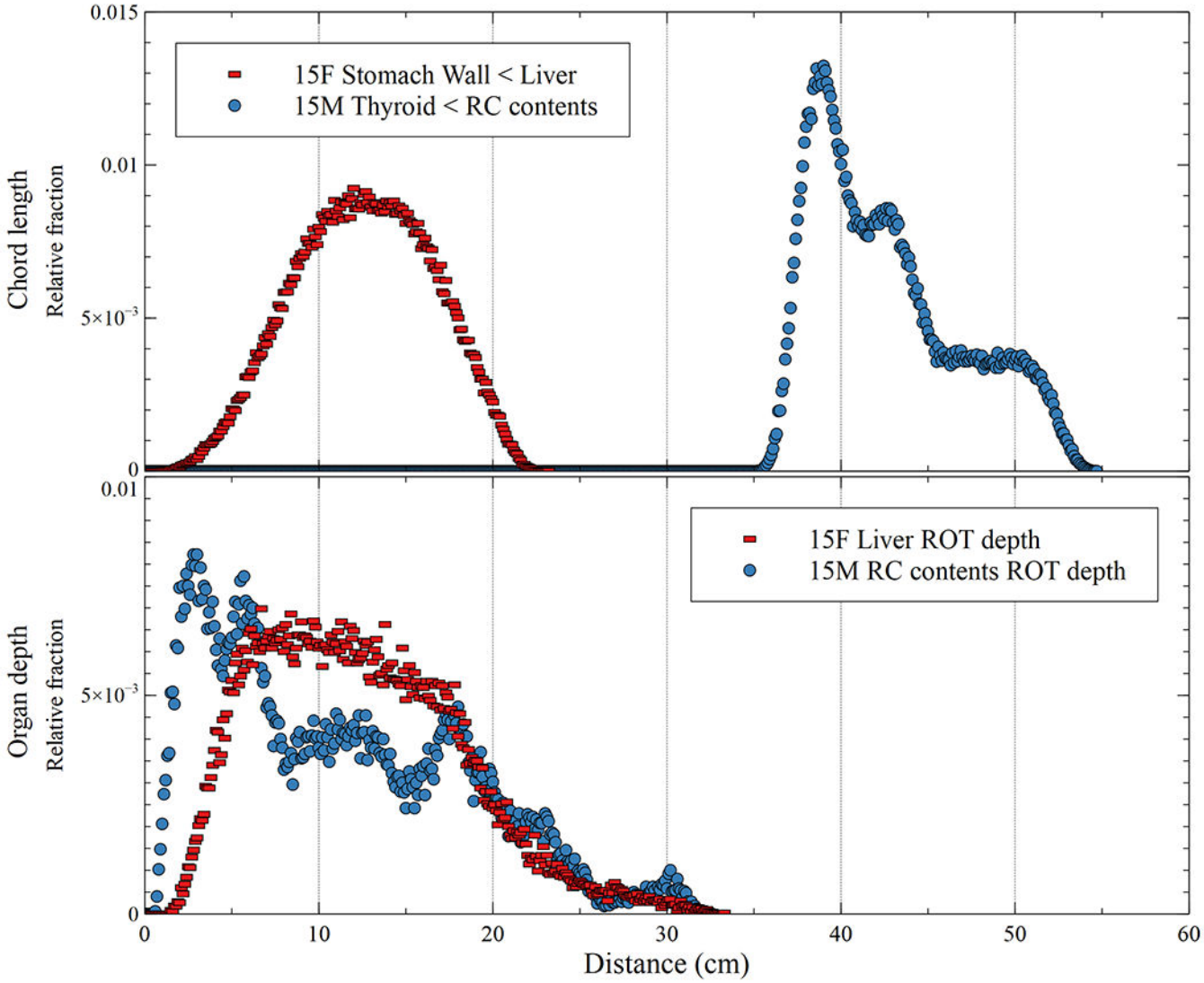

Figure 4:

Chord length distance distributions for the 15-year-old female liver source to stomach wall target and 15-year-old male right colon (RC) contents source to thyroid target (top); distributions of organ depth to the surface of the body (ROT depth) for the 15-year-old female liver and 15-year-old male RC contents (bottom).

Table 1:

Overview of the source sampling techniques used to calculate SAFs for the bone and blood source regions of the ICRP phantoms.

Source region	Sampling information
Blood	45.5% of blood volume in each ICRP phantom is segmented (e.g., blood vessels) and the rest is dispersed throughout the rest of the body, excluding bone mineral. The blood source SAF is estimated through simulation of the segmented blood as a source term; the resulting SAF is then combined with the SAFs for the other organs of the body, weighted based on each organ's proportion of total blood volume as given by Table 4.3 of ICRP Publication 143.
Cortical bone mineral surface/volume *	Cortical bone mineral is contained within the segmented cortical bone structures of the ICRP phantoms. Uniform sampling of these segmented voxels creates this source term.
Trabecular bone mineral surface/volume *	Segmented trabecular bone (spongiosa) contains both mineral and marrow. Fractions of the total trabecular bone volume at each bone site are given by Tables 3.3-3.8 of ICRP Publication 143; for this source, bone sites are sampled based on these fractions.
Cortical bone marrow	Cortical bone marrow is contained within the segmented medullary cavities of the ICRP phantoms. Uniform sampling of these segmented voxels creates this source term.
Trabecular bone marrow	Segmented trabecular bone (spongiosa) contains both mineral and marrow. Fractions of the total active marrow at each bone site are given by Tables 3.3-3.8 of ICRP Publication 143; for this source, spongiosa bone sites were sampled based on their contained fraction out of total trabecular active marrow (not including medullary cavities).
Red (active) bone marrow	Active marrow SAFs are a weighted combination of the cortical bone marrow and trabecular bone marrow SAFs, based on the proportion of active marrow in the cortical and trabecular bones out of total active marrow in the phantom.
Yellow (inactive) bone marrow	Fractions of the total inactive marrow at each bone site are given by Tables 3.3-3.8 of ICRP Publication 143; for this source, bone sites are sampled based on these fractions.

* No distinction is made between surface and volume source terms in the whole-body voxel phantoms of ICRP Publication 143, which is appropriate for long-range radiations such as neutrons. For short-ranged radiations (alphas and electrons), separate skeletal models are used to distinctly model these source regions.

Table 2:

Spontaneous fission neutron SAF scaling factors used to extend ^{252}Cf SAFs to each of the other 27 spontaneous fission neutron emitters based on the radionuclide-specific soft tissue KERMA coefficient (Gy cm^2) and average spontaneous fission neutron energy ($\bar{E}$). Spectral-averaged radiation weighting factors, w_R, and branching fractions (B.F.) for spontaneous fission are also shown.

					Normalization to ^{252}Cf		
Nuclide	**B.F.**	**w_R**	**KERMA**	**$\bar{E}$ (MeV)**	**KERMA**	**$\bar{E}$**	**Factor**
^{238}U	5.45x10^{-7}	17.495	2.58x10^{-11}	1.688	0.878	1.365	**1.198**
^{236}Pu	1.37x10^{-9}	16.667	2.90x10^{-11}	2.24	0.988	1.029	**1.017**
^{238}Pu	1.85x10^{-9}	16.988	2.78x10^{-11}	2.021	0.947	1.141	**1.08**
^{240}Pu	5.75x10^{-8}	17.119	2.73x10^{-11}	1.933	0.93	1.192	**1.108**
^{242}Pu	5.54x10^{-6}	17.074	2.75x10^{-11}	1.961	0.935	1.175	**1.099**
^{244}Pu	1.21x10^{-3}	17.374	2.63x10^{-11}	1.766	0.895	1.305	**1.168**
^{240}Cm	3.9x10^{-8}	16.468	2.98x10^{-11}	2.382	1.013	0.968	**0.981**
^{242}Cm	6.37x10^{-8}	16.877	2.83x10^{-11}	2.097	0.962	1.099	**1.058**
^{244}Cm	1.37x10^{-6}	16.855	2.84x10^{-11}	2.111	0.965	1.092	**1.053**
^{245}Cm	6.10x10^{-9}	16.84	2.84x10^{-11}	2.121	0.966	1.087	**1.05**
^{246}Cm	2.63x10^{-4}	16.92	2.81x10^{-11}	2.067	0.956	1.115	**1.066**
^{248}Cm	8.39x10^{-2}	17.088	2.74x10^{-11}	1.954	0.934	1.18	**1.102**
^{250}Cm	7.40x10^{-1}	17.269	2.67x10^{-11}	1.835	0.909	1.256	**1.142**
^{246}Cf	2.50x10^{-6}	16.569	2.94x10^{-11}	2.31	1.001	0.998	**0.999**
^{248}Cf	2.90x10^{-5}	16.561	2.95x10^{-11}	2.316	1.002	0.995	**0.997**
^{249}Cf	5.02x10^{-9}	16.569	2.94x10^{-11}	2.31	1.001	0.998	**0.999**
^{250}Cf	7.70x10^{-4}	16.569	2.94x10^{-11}	2.31	1.001	0.998	**0.999**
^{252}Cf	3.09x10^{-2}	16.575	2.94x10^{-11}	2.306	1	1	**1**
^{254}Cf	9.97x10^{-1}	16.569	2.94x10^{-11}	2.31	1.001	0.998	**0.999**
^{253}Es	8.90x10^{-8}	17.02	2.78x10^{-11}	2.003	0.945	1.151	**1.087**
^{254}Es	3.00x10^{-8}	17.02	2.78x10^{-11}	2.003	0.945	1.151	**1.087**
^{254m}Es	4.50x10^{-4}	17.02	2.78x10^{-11}	2.003	0.945	1.151	**1.087**
^{255}Es	4.50x10^{-5}	17.02	2.78x10^{-11}	2.003	0.945	1.151	**1.087**
^{252}Fm	2.30x10^{-5}	17.02	2.78x10^{-11}	2.003	0.945	1.151	**1.087**
^{255}Fm	2.30x10^{-7}	17.02	2.78x10^{-11}	2.003	0.945	1.151	**1.087**
^{256}Fm	9.19x10^{-1}	17.02	2.78x10^{-11}	2.003	0.945	1.151	**1.087**
^{257}Fm	2.10x10^{-3}	17.02	2.78x10^{-11}	2.003	0.945	1.151	**1.087**

Table 3:

Validation results of the point kernel methodology for the 15-year-old male and female phantoms. Chord length calculations provide the source-target separation, which are used with one of five kernels to convert distance to SAF. The choice in kernel is based on the 25th percentile depth of the source region from the surface of the body. The kernel SAFs for ^{252}Cf are compared against those which have already been found through full MC simulation.

	Region*		Chord length (cm)			Source region depth (cm)		SAF comparison (kg^{-1})			
Phantom	**Target**	**Source**	**Min**	**Median**	**Max**	**25th percentile**	**Kernel offset**	**Kernel SAF**	**MCNP SAF**	**MC Error**	**% difference**
15f	LC-stem	LC-cont	0.1	7.5	15.1	3.6	12	6.93x10^{-1}	6.28x10^{-1}	<0.1%	10%
	St-stem	Liver	0.8	12.6	22.6	7.8	6	5.05x10^{-2}	4.83x10^{-2}	0.1%	5%
	Ht-wall	St-cont	4.9	14	25.6	8	6	2.00x10^{-2}	2.18x10^{-2}	0.2%	−8%
	Oesophagus	Kidneys	4.2	20.7	39.9	5.3	9	1.18x10^{-2}	1.12x10^{-2}	0.6%	5%
	Pancreas	Ovaries	17.4	21.6	27.4	10.8	3	3.48x10^{-3}	3.74x10^{-3}	0.7%	−7%
	RC-stem	Lungs	13.6	30.3	49.2	8.5	6	1.58x10^{-3}	1.39x10^{-3}	1.1%	13%
	Brain	RC-cont	43.3	56.7	72.1	4.5	9	8.43x10^{-5}	7.05x10^{-5}	2.0%	20%
15m	GB-wall	Testes	27.5	31.6	35.3	3.3	12	7.12x10^{-4}	7.55x10^{-4}	1.2%	−6%
	Liver	Liver	0.1	7.6	21.5	7.3	9	2.29x10^{-1}	2.11x10^{-1}	<0.1%	9%
	SI-stem	St-cont	0.7	13.3	27.4	7.8	6	3.90x10^{-2}	3.70x10^{-2}	0.1%	5%
	Ht-wall	Kidneys	10.2	21.2	33.7	6.5	9	4.99x10^{-3}	5.61x10^{-3}	<0.1%	-11%
	Testes	SI-cont	6.7	19.2	33.8	8.6	6	1.03x10^{-2}	9.48x10^{-3}	1.0%	9%
	Thyroid	RC-cont	35.2	41.7	54.6	4.9	9	2.49x10^{-4}	2.13x10^{-4}	8.2%	17%
	UB-wall	Lungs	29.2	43.1	57.4	8.5	6	3.28x10^{-4}	2.79x10^{-4}	3.6%	18%

*Abbreviations of source and target regions are defined within Annex A of ICRP Publication 133.

Table 4:

Validation results of the extension of ^{252}Cf SAFs to those for other spontaneous fission neutron emitters in the ICRP reference 5-year-old male phantom. Scaling factors from Table 2 adjust the SAFs for ^{252}Cf to estimate those for ^{238}U and ^{244}Pu. These extended SAFs for ^{238}U and ^{244}Pu are compared against those which were found through a full MC simulation of the liver, cortical bone, and trabecular bone source regions.

	Region*		SAF (kg^{-1}) comparison				
Radionuclide	**Target**	**Source**	**^{252}Cf SAF**	**Scaling factor**	**Weighted SAF**	**MCNP SAF**	**% difference**
^{238}U	Thyroid	Liver	6.19×10^{-3}	1.198	7.41×10^{-3}	6.50×10^{-3}	14%
	Liver	Liver	3.94×10^{-1}		4.72×10^{-1}	4.64×10^{-1}	2%
	St-stem	C-bone	9.48×10^{-3}		1.14×10^{-2}	1.04×10^{-2}	9%
	UB-wall	C-bone	2.18×10^{-2}		2.61×10^{-2}	2.47×10^{-2}	6%
	LC-stem	T-bone	9.58×10^{-3}		1.15×10^{-2}	1.05×10^{-2}	9%
	Oesophagus	T-bone	4.04×10^{-2}		4.84×10^{-2}	4.61×10^{-2}	5%
^{244}Pu	Ht-wall	Liver	8.47×10^{-2}	1.168	9.89×10^{-2}	9.48×10^{-2}	4%
	Spleen	Liver	2.18×10^{-2}		2.55×10^{-2}	2.38×10^{-2}	7%
	Prostate	C-bone	2.24×10^{-2}		2.61×10^{-2}	2.48×10^{-2}	5%
	SI-stem	C-bone	1.14×10^{-2}		1.33×10^{-2}	1.24×10^{-2}	7%
	R-marrow	T-bone	7.13×10^{-2}		8.33×10^{-2}	8.24×10^{-2}	1%
	Testes	T-bone	1.00×10^{-2}		1.17×10^{-2}	1.10×10^{-2}	6%

*Abbreviations of source and target regions are defined within Annex A of ICRP Publication 133.

Table 5:

Relative fractional absorbed dose contributions to the liver of the ICRP male reference phantoms from the emissions of a uniform ^{252}Cf burden.

	Radiation Fractional Absorbed Dose Contribution (%)					
Radiation	**Newborn**	**1 y old**	**5 y old**	**10 y old**	**15 y old**	**Adult**
Gamma rays	$< 10^{-3}$	$< 10^{-3}$	$< 10^{-3}$	$< 10^{-3}$	$< 10^{-3}$	$< 10^{-3}$
X rays	0.001	0.002	0.003	0.004	0.007	0.009
IC electrons	0.036	0.036	0.036	0.036	0.036	0.036
Auger electrons	0.001	0.002	0.003	0.005	0.008	0.011
Alpha particles	49.758	49.667	49.538	49.477	49.305	49.319
Alpha recoil	0.803	0.802	0.800	0.799	0.796	0.796
Fission fragments	48.863	48.774	48.647	48.588	48.419	48.432
Neutrons	0.501	0.632	0.814	0.860	1.057	0.882
Prompt gamma	0.018	0.041	0.076	0.111	0.178	0.246
Delayed gamma	0.019	0.045	0.083	0.121	0.195	0.269
Delayed beta	1.804	1.874	1.903	1.895	1.928	1.910
Dose (Gy/n.t.)	$1.14x10^{-11}$	$4.90x10^{-12}$	$2.64x10^{-12}$	$1.81x10^{-12}$	$1.13x10^{-12}$	$8.15x10^{-13}$